Industrial IoT Based Condition Monitoring for Wind Energy Conversion System

Md Liton Hossain, Ahmed Abu-Siada, S. M. Muyeen, Md Mubashwar Hasan, and Md Momtazur Rahman

***Abstract*—Wind energy has been identified as the second dominating source in the world renewable energy generation after hydropower. Conversion and distribution of wind energy has brought technology revolution by developing the advanced wind energy conversion system (WECS) including multilevel inverters (MLIs). The conventional rectifier produces ripples in their output waveforms while the MLI suffers from voltage balancing issues across the DC-link capacitor. This paper proposes a simplified proportional integral (PI)-based space vector pulse width modulation (SVPWM) to minimize the output waveform ripples, resolve the voltage balancing issue and produce better-quality output waveforms. WECS experiences various types of faults particularly in the DC-link capacitor and switching devices of the power converter. These faults, if not detected and rectified at an early stage, may lead to catastrophic failures to the WECS and continuity of the power supply. This paper proposes a new algorithm embedded in the proposed PI-based SVPWM controller to identify the fault location in the power converter in real time. Since most wind power plants are located in remote areas or offshore, WECS condition monitoring needs to be developed over the internet of things (IoT) to ensure system reliability. In this paper, an industrial IoT algorithm with an associated hardware prototype is proposed to monitor the condition of WECS in the real-time environment.**

***Index Terms*—Asset management, condition monitoring, fault diagnosis, industrial internet of things (IoT), wind energy conversion system.**

I. Introduction

WITH the rapid growth of the world's population, energy consumption is increasing on a daily basis which boosts energy production demands. To meet such power demands, pressure for the utilization of fossil fuels, petroleum, coal and natural gas have been increased [1]. However, the excessive use of fossil fuels to produce worldwide energy is responsible for adverse environmental effects including skin cancer, global warming, acid rain and air pollution [2]. These serious environmental consequences have encouraged scientists and engineers to search for alternate sources of energy. Renewable energy sources, such as hydro, wind, solar and biothermal, are the most predominant sources nowadays, as they are infinite, cost-effective, and environmentally safe [3]. Wind energy is identified as the second dominating renewable energy source after the hydropower generation since it contributed 6% of the total world electricity generation in the year 2019 [4]–[6].

According to the Australian government energy statistics, renewable energy generation shares in 2018 were 21% of the nation energy production, while it was 17.3% in the year 2016 [7]. According to statistics from the world energy agency in 2018, wind energy contributed 4% of the total global energy generation, while this is forecasted to triple by the year 2024 [8]. However, to implement this ambitious forecast, several challenges need to be overcome by designing the proper WECS mechanical, electrical and control systems including turbine blades, gearboxes, drivetrains, generators and power converters [9], [10]. With the advancement in technologies, WECS capacity has significantly increased in the last few years. While such large capacity may have some advantageous in reducing the space of wind farm installations, it raises challenges in monitoring the WECS health conditions in real-time to avoid catastrophic consequences. Various combinations of generators and power electronic converters (PECs) with different control techniques have been developed to achieve the desired rate for full variable operation of WECS, which increases its efficiency and reduces mechanical stress on wind turbine blades and drivetrains and improves grid power quality [11].

The PEC has been given much attention due to its flexibility and rapid response which facilitates the integration of various renewable energy sources to power grids and improves power system reliability [12]–[14]. Various PEC control topologies have been proposed to suit several applications, such as battery energy storage [15]–[17], photovoltaic systems [18], [19], electric vehicles [20], [21], and power conditioning [22]. The PEC consists of a rectifier and inverter. The rectifier converts AC power input to intermittent DC power while the inverter converts the intermittent DC power to AC output power. The rectifier produces low frequency harmonic ripples in the intermittent DC power which is quite a challenging task to minimize [23]. Using a bulky electrolytic capacitor to suppress such ripples restricts the efficiency and power density of the converter. Authors of [24] presented a controller to eliminate such voltage ripples. However, the rectifier exhibits poor dynamic performances due to the low bandwidth of the controller during ripples' suppression. Authors of [25]

Manuscript received March 9, 2020; revised June 4, 2020; accepted June 24, 2020. Date of online publication October 6, 2020; date of current version November 30, 2020.

M. L. Hossain (corresponding author, e-mail: mdliton.hossain@postgrad.curtin.edu.au; ORCID: https://orcid.org/0000-0001-9393-6534), A. Abu-Siyada, S. M. Muyeen and M. M. Hasan are with Department of Electrical and Computer Engineering, Curtin University, Perth, Australia.

M. M. Hasan is with School of Science, Engineering and IT, Federation University, Australia.

M. M. Rahman is with Edith Cowan University, Australia.

DOI: 10.17775/CSEEJPES.2020.00680

proposed an optimised design for the PEC with extended controller bandwidth. In addition, a new discrete function minimization technique has been presented to avoid current distortion, maintain unity power factor operations and achieve better dynamic response [26]. A pulse width modulation (PWM) controller has been employed to suppress the ripples of the output voltage of a buck single-stage bi-directional AC/DC converter [27]. In this technique, minimum commutations have been maintained to guarantee the closeness of the three voltage levels to the output reference voltage, hence minimizing the output voltage ripples.

Advancement in control systems has brought revolution in the area of high-power medium-voltage MLI. The MLIs have several advantages over conventional inverters that include less stress on switching devices, more utilization of the DC-link power, and better power quality [28]. However, MLI exhibits some drawbacks such as voltage balancing issues along with the complexity of the used hardware and software. A voltage-balancing controller based on logic function is proposed to reduce the voltage ripples and balance the voltage across the capacitors of modular multilevel power converters [29]. Authors of [30] presented a controller based on a flexible AC transmission system (FACTS) for cascaded MLI to balance the voltages across the capacitor and maintain the average value of the DC-link voltage at a constant level. It should be noted that neutral point clamped inverters (NPCIs) also suffer from a voltage balancing issue. The unbalanced neutral point voltage leads to unbalance in the DC-link voltage and vice versa. A sine PWM controller associated with the phase shift technique is presented in [31] to balance the neutral point voltage as well as capacitors voltages of the NPCI.

Another issue associated with the PEC is the various faults it may exhibit during its operation. Faults, such as open and short circuit faults of switching devices and DC-link capacitors interrupt the continuity of the power flow. Switching devices and capacitors are the most fragile elements in power electronic conversion systems [32], [33]. As reported in a survey conducted on over 200 products from 80 different companies, capacitor and semiconductor switch failures account for 30% and 21% of power converter failures, respectively [34]. In addition, about 20% of the malfunctions within WECS are due to failures in the power electronic converters [35]. If these faults are not detected and rectified at the early stages, they may lead to catastrophic consequences and loss of revenue. As such, more systematized operation and maintenance schemes are required to ensure the reliability of the WECS.

Since most wind power plants are located in remote areas or offshore in harsh weather and operating conditions, a reliable online condition monitoring and fault diagnosis technique needs to be developed to monitor the condition of the WECS in real-time to ensure system reliability. Online condition monitoring has brought about tremendous changes to industrial applications, where remote users can monitor the condition of industrial devices over the internet of things (IoT) [36]. International Data Corporation identified that spending on IoT and its related projects in the period 2016–2022, will go beyond AUD $6 trillion [37]. However, there have been several challenges to develop industrial IoT projects, such as data encryptibility, security, privacy, etc. To overcome such challenges, there are more than 123 standards and technologies published in literature, which need to be strictly maintained, that deal with the development of IoT projects [38]. The standards of internet protocols are primarily divided into three categories, such as wireless personal area networks (WPANs), wireless local area networks (WLANs) and cellular networks [39]. The WPAN uses low rate standards (IEEE 802.14.4) and the WLAN has a limited bandwidth standard (IEEE 802.3). Cellular networks, such as second-generation (2G), third-generation (3G), fifth-generation (5G), Long-term Evolution (LTE), worldwide interoperability for microwave (WiMAX), general packet radio service (GPRS) and global systems for mobile communication (GSM) have fast data rates, wide coverage, and appropriate bandwidth, which is becoming the mainstream of industrial IoT. Global systems for mobile communication (GSM) and general packet radio service (GPRS) are promising techniques to monitor the conditions of WECS.

From the above discussion, the main contributions of this paper can be summarized as follows:

- Proposing a new PI-based SVPWM controller to suppress the ripples of the converter DC-link voltage and resolving the voltage balancing issues across the DC-link capacitors.
- Developing an embedded algorithm to monitor the condition of DC-link capacitors and switching devices of the power converters of WECS.
- Proposing an industrial IoT algorithm associated with hardware prototypes to monitor the condition of WECS in real time.

II. Proposed PI-Based SVPWM Controller and Industrial IoT Algorithm for WECS

A block diagram of the WECS is depicted in Fig. 1 which comprises the proposed PI-based SVPWM controller and industrial IoT hardware prototype.

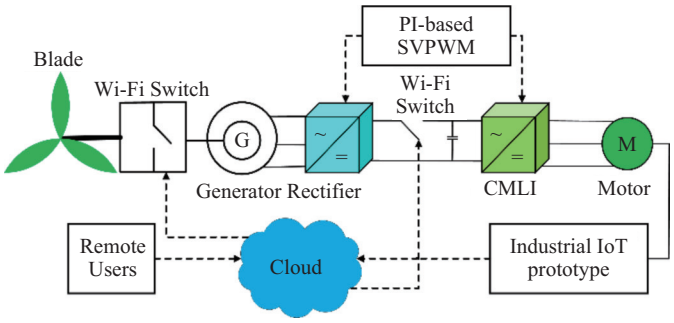

Fig. 1. Block diagram of the proposed controller and IoT for WECS.

Three-phase instantaneous AC phase voltages generated by the WECS are given by:

$$V_{\text{an}} = v_{\text{m}} \sin \omega t \tag{1}$$

$$V_{\text{bn}} = v_{\text{m}} \sin \left(\omega t - \frac{2\pi}{3} \right) \tag{2}$$

$$V_{\rm cn} = v_{\rm m} \sin\left(\omega t + \frac{2\pi}{3}\right) \tag{3}$$

The instantaneous phase voltages are converted into an intermittent DC-link voltage across the DC-link capacitors $V_{\rm dc}$ through six bi-directional switching devices as given in (4).

$$V_{\rm dc} = \frac{1}{\pi}\int_0^{\pi} v_{\rm m} \sin\omega t {\rm d}(\omega t) = \frac{2v_{\rm m}}{\pi} \tag{4}$$

The proposed PI-based space vector pulse width modulation (SVPWM) is designed as shown in Fig. 2. In this technique, output currents and voltages are measured and transformed to the dq-reference frame using Clarke and Park's transformation. The dq-reference signal ($I_{\rm ref}$) is compared to the DC-link current ($I_{\rm dc}$) and the error signal is fed to the PI controller as per the equations below.

$$I_{\rm ref} = I_r \sin\omega t \tag{5}$$

$$I_{\rm d\_con} = k_{\rm p}\left(I_{\rm d} - I_{\rm ref}\right) + k_i \int \left(I_{\rm d} - I_{\rm ref}\right) {\rm d}t \tag{6}$$

$$I_{\rm q\_ref} = 0$$

$$I_{\rm q\_con} = k_{\rm p}\left(I_{\rm q} - I_{\rm q\_ref}\right) + K_i \int \left(I_{\rm q} - I_{\rm q\_ref}\right) {\rm d}t \tag{7}$$

$$I_{\alpha i} = I_{\rm d\_con}\left(\cos\theta - I_{\rm q\_con}\sin\theta\right) \tag{8}$$

$$I_{\beta i} = I_{\rm d\_con}\left(\sin\theta + I_{\rm q\_con}\cos\theta\right) \tag{9}$$

A conventional 2-level space vector diagram is a hexagon which is divided into six sectors. Each sector consists of an equilateral triangle of a unity side and height ($h = \sqrt{3}/2$) [40]. The diagram comprises m^3 switching states represented in the reference frame, where m is the number of levels in the output voltage waveform. The angle (θ_i), and magnitude (I_i^*) are determined from the following equations.

$$\theta_i = \tan^{-1}\left(\frac{{\rm I}_{\beta i}}{{\rm I}_{\alpha i}}\right) \tag{10}$$

$$I_i^* = \sqrt{{\rm I}_{\alpha i}^2 + {\rm I}_{\beta {\rm i}}^2} \tag{11}$$

The sector number (s) is determined by:

$$s = {\rm floor}\ \left(\frac{\theta_i}{\pi/3}\right) + 1 \tag{12}$$

The conventional space vector diagram has been extended to a multilevel space vector diagram [41] which is divided into six sectors with $(m-1)^2$ number of triangles and m^3 switching vectors in each sector.

A conventional five level space vector diagram is shown in Fig. 3. The 5-level space vector diagram contains 16 triangles in each sector and 125 switching vectors. Triangle-1 has 13 different switching vectors; (000, 100, 110, 111, 211, 221, 222, 322, 332, 333, 433, 443, 444). Triangle-2 has 10 different switching vectors; (100, 200, 210, 211, 311, 321, 322, 422, 432, 433). Triangle-3 has 11 switching vectors; (100, 110, 210, 211, 221, 321, 322, 332, 422, 423, 433). Triangle-4 has 10 different switching vectors; (110, 210, 220, 221, 321, 331, 332, 432, 442, 443). Triangle-5 has 7 different switching vectors; (200, 300, 310, 311, 411, 421, 422). Triangle-6 has 8 different switching vectors; (200, 210, 310, 311, 321, 421, 422, 432). Triangle-7 has different switching vectors; (210, 310, 320, 321, 421, 431, 432). Triangle-8 has 8 different switching vectors; (210, 220, 320, 321, 331, 431, 432, 442). Triangle-9 has 7 different switching vectors; (220, 320, 330, 331, 431, 441, 442). Triangle-10 has 4 different switching vectors; (300, 400, 410, 411). Triangle-11 has 5 different switching vectors; (300, 310, 410, 411, 421). Triangle-12 has 4 different switching vectors; (310, 410, 420, 421). Triangle-13 has 5 different switching vectors; (310, 320, 420, 421, 431). Triangle-14 has 4 different switching vectors; (320, 420, 430, 431). Triangle-15 has 5 different switching vectors; (320, 330, 430, 431, 441) and triangle-16 has 4 different switching vectors (330, 430, 440, 441). As can be seen, the complexity of a 5-level SVPWM is due to the large number of switching vectors. Moreover, triangles exhibit unequal numbers of switching vectors which causes a voltage imbalance across the DC-link capacitors. Vectors (000 to 111) basically contribute to the performances of the conventional 2-level space vector while vectors (111 to 222), (222 to 333) and vectors (333 to 444) are respectively contributing to the performances of 3-level, 4-level and 5-level space vectors.

In this paper, the switching vectors for 2-level and 4-level are omitted. This will not only reduce the complexity of the switching vectors but will also balance the voltages across the DC-link capacitors. It is to be noted that omitting such low level contributed switching vectors does not significantly affect the performances of the CMLI.

This is attributed to the fact that low level contributed switching vectors are of least contribution to the performance of the inverter while the switching vectors of high-level contribution dominate the CMLI performance. The conventional space vector diagram as shown in Fig. 3 consists of three types of switching vectors marked by three different color bands (red, blue and green).

The switching vectors marked by the red color band, such as (000, 100, 110, 111, 211, 221, 222) of triangle-1 and (100, 200, 210, 211) of triangle-2 of sector-1 are completely redundant. The green color-coded switching vectors such as (333, 433, 443, 444) of triangle-1 and (422, 432, 433) of triangle-2 of sector-1 are mandatory for the formation of triangles.

The blue color-coded switching vectors e.g., (322) are redundant for triangle-1 but mandatory for triangle-2 of sector-1. In a similar way, it can be concluded that the green color-coded switching vectors are mandatory for the formation of triangles while the red color-coded switching vectors are completely redundant and the blue color-coded ones are either redundant or mandatory for the formation of triangles of the space vector diagram. Hence, the 5-level space vector diagram is simplified by omitting red color-coded switching vectors as presented in Fig. 4. The proposed simplified diagram comprises 98 switching vectors instead of 127 switching vectors of the conventional space vector diagram. Moreover, only four switching vectors are enough to create a triangle. The elimination process of low weighted switching vectors for triangle-1 is shown in Fig. 5. These four high weighted switching vectors are selected from the simplified diagram to implement the MLI control pulses.

The PEC suffers from various types of faults which interrupt the continuity of power flow. The proposed algorithm to facil-

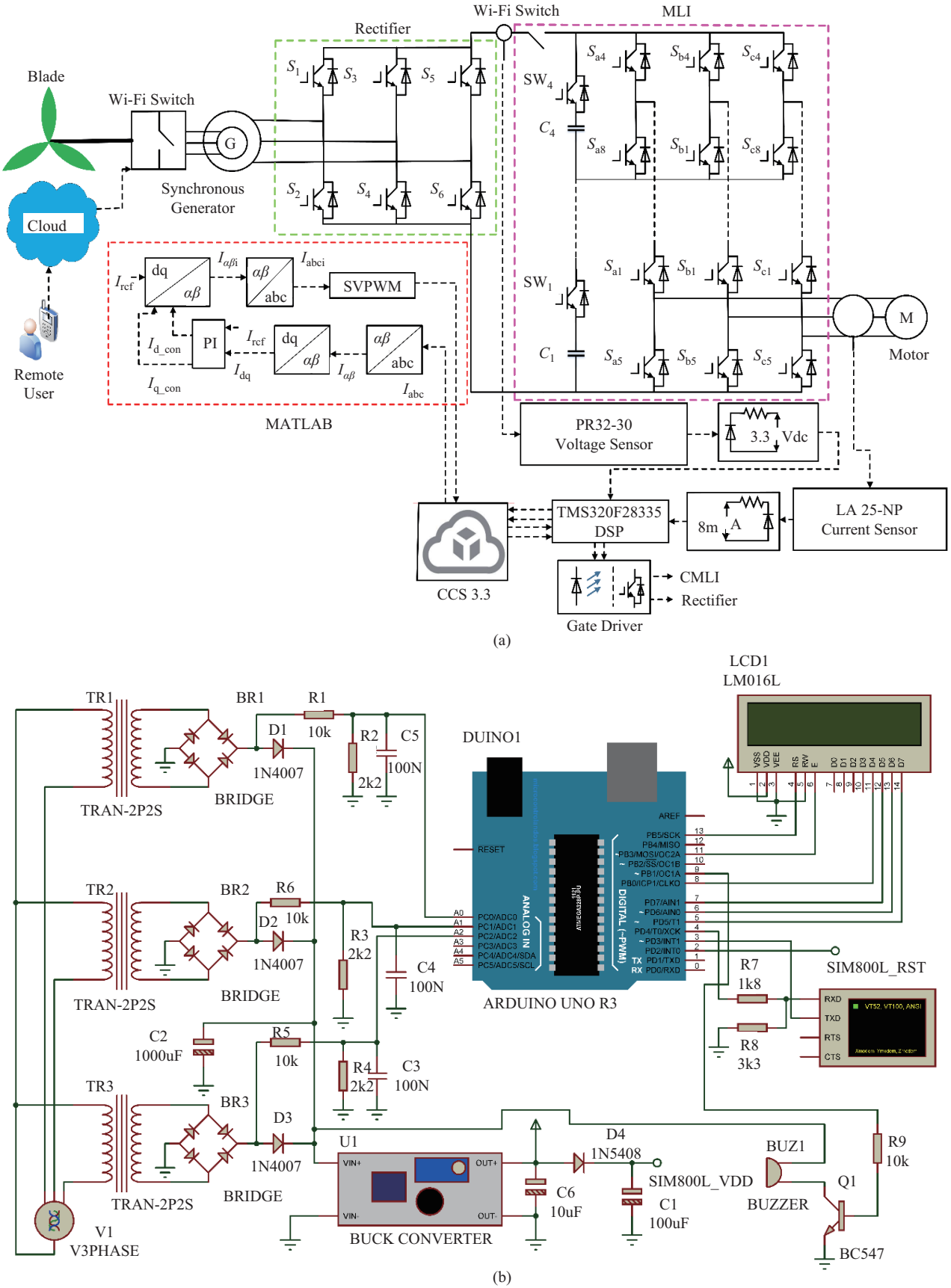

Fig. 2. Proposed systems for WECS (a) PI-based SVPWM (b) industrial IoT.

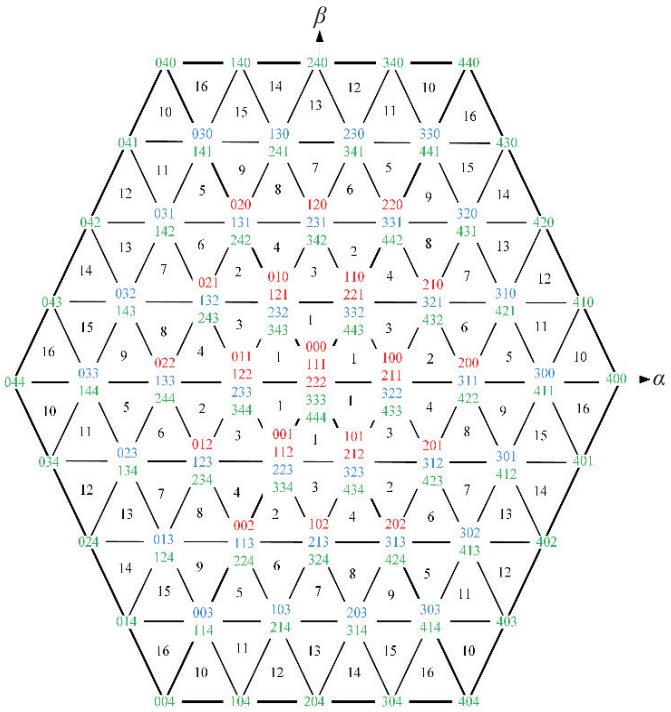

Fig. 3. Conventional five-level space vector diagram.

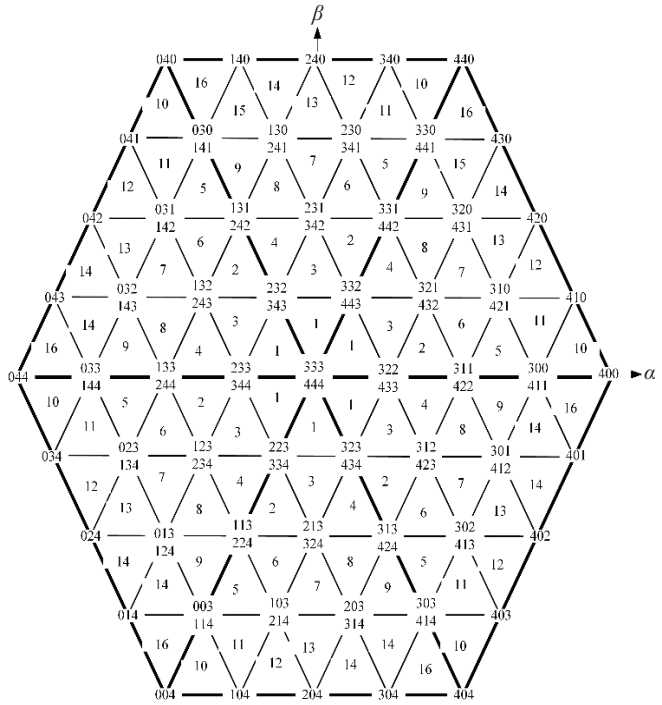

Fig. 4. Proposed five-level space vector diagram.

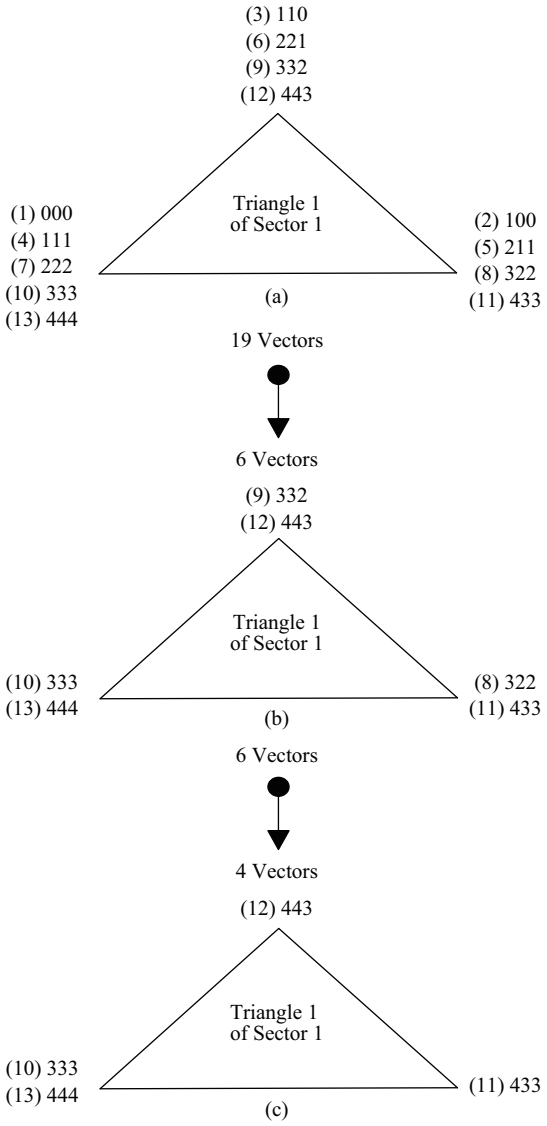

Fig. 5. Process of omitting low weighted switching vectors for triangle-1.

itate reliable condition monitoring of the switching devices of the three-phase cascaded MLI and DC-link capacitor in real-time is shown in Fig. 6.

The PI-based SVPWM generates four control pulses for the switching devices (S1 to S4); each runs for 270 s. The algorithm shown in Fig. 6 is designed to continuously monitor the condition of the MLI switches over this interval. A counter is used to record the timing period. An additional switch is connected to the output of each control pulse. All additional four switches are turned on during healthy conditions of the switching devices. When a fault in S1 is sustained for a period of more than 30 s, the first additional switch will be turned off and generates a faulty control pulse until the counter reaches 60 s. The same procedure is adopted for faults in the other switches. A programmable relay can be utilized to implement this control scheme.

Due to the faulty control pulses, three modes can be observed in the RMS output waveforms of the inverter. It is assumed that, all switches are in healthy condition for 30 s. At $t = 30$ s, a fault is simulated in the inverter switches and at $t = 90$ s, the fault is cleared. The same scenario is assumed for all the upper switching devices (S_{a1} to S_{a4}) of the three-phase MLI.

In addition, the proposed PI-based SVPWM embedded algorithm is applied to monitor the open and short circuit faults in the DC-link capacitors as presented in Fig. 6. The generated

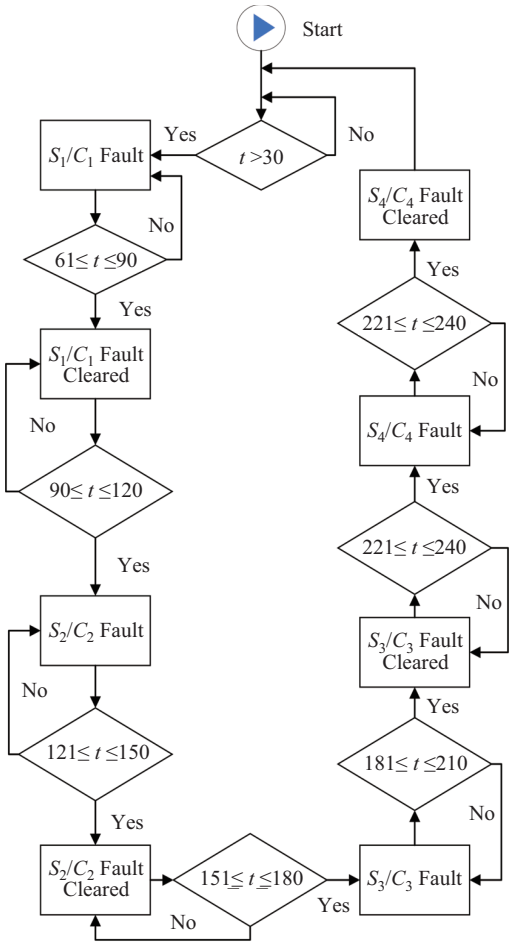

Fig. 6. Proposed PI-based space vector pulse width modulation algorithm.

fault control pulses are applied to control the DC-link switches (SW1 to SW4). These signals trigger three modes in the RMS output waveforms of the inverter as well, and will be elaborated upon in the results below.

The proposed industrial IoT algorithm is presented to monitor the condition of the DC-link capacitor and switching devices in real time. The algorithm is divided into a data sensing layer, data processing layer, data link layer, network layer, network layer, and application layer. The data sensing layer consists of a three-phase step down transformer and three-phase full-bridge rectifier as shown in Fig. 2(b). The three-phase voltages are captured from the three-phase cascaded MLI. These three-phase voltages are fed to the three-phase full-bridge rectifier through a three-phase step down transformer. The DC output voltage of the three-phase bridge rectifier $= 1/\pi \int_0^{\pi} v_{\mathrm{m}}^{*} \sin \omega t \mathrm{d}(\omega t)$ is fed to the data processing layer which consists of an Arduino Uno board along with an integrated development environment (IDE), and a liquid crystal display (LCD). The data is processed in a binary form after which it is transferred to the data link layer. The data link layer consists of a global system for mobile (GSM) module (SIM Card), SIM800L module, and a global packet radio service (GPRS).

The SIM800L module can work as a cellular mobile phone with the integration of external peripheral, which can generate calls, SMS, email and build dual communication with the internet. Data can be written to the internet and the web page can be read through the SIM800 module.

UART (Universal Asynchronous Receiver/Transmitter) sends (T_X for SIM800 and D_8 for Arduino Uno) and receives (R_X for SIM800 and D_7 for Arduino Uno) lines. The required hardware components and software to develop the proposed Industrial IoT system comprises SIM800L, Arduino Uno, a SIM800L device, and a USB cable for serial interface between the Arduino and computer.

A program is developed in the Arduino IDE environment to control the data processing and send it to the SIM800 module along with the GSM module via the Arduino Uno board which is described below.

In the Arduino IDE, three libraries; Adafruit FONA Library (AFL), Software Serial Library (SSL), and Liquid Crystal Library (LCL) are included. The AFL is used for GSM Breakouts. The Arduino hardware has a built-in support for serial communication using SSL on pins 0 and 1, which is also transmitted to the computer via a USB connection. The SSL has been developed to allow serial communication on other digital pins of the Arduino. The LCL allows the Arduino Uno board to print message signals in an LCD display.

The posted data in the server are compared with a threshold voltage (v_{th}). If the posted data $\leqslant v_{\mathrm{th}}$, a message signal is generated and sent to the application layer. The application layer consists of authenticated remote users, email servers and wi-fi switches so that authenticated remote users can access data in real time. A brief flow chart of the proposed Industrial IoT for WECS is shown in Fig. 7.

III. Results and Discussion

The proposed PI-based SVPWM is designed and simulated in the MATLAB software environment. The blade length, wind speed, tip speed ratio, and power co-efficient are set to 26 m, 12 m/s, 8 and 0.48; respectively. Three-phase output voltages of the wind generator are converted into DC-link voltage as shown in Fig. 8(a). The DC-link voltage is inverted to a three-phase AC voltage using the three-phase cascaded MLI as shown in Fig. 8(b). The sampling frequency for both the rectifier and the three-phase cascaded MLI is set to 5 kHz. From the simulation results, it can be concluded that the proposed PI-based SVPWM controller can minimize the ripples in the generated waveforms.

An experimental setup is developed to validate the simulation results as depicted in Fig. 9. The experimental prototype consists of a synchronous generator, insulated gate bipolar transistor (IGBT, Dual N Channel, 155 A, 2 V, 511 W, 1.2 kV), voltage sensor (PR32-30), current sensor (LA 25-NP), digital signal processing board (TMS320F28335), 3-phase squirrel cage induction motor (380 V, 1.6/3.1A, 0.4/1KW, 0.64/0.76), 3-phase gate driver (5/15 V), and DC supply (GPC-3030D, 0/30 V, 0/3A).

To validate the feasibility of the proposed controllers and condition monitoring techniques, experimental measurements are carried out on a laboratory test-rig as shown in Fig. 9. The proposed PI-based SVPWM controller is uploaded to a

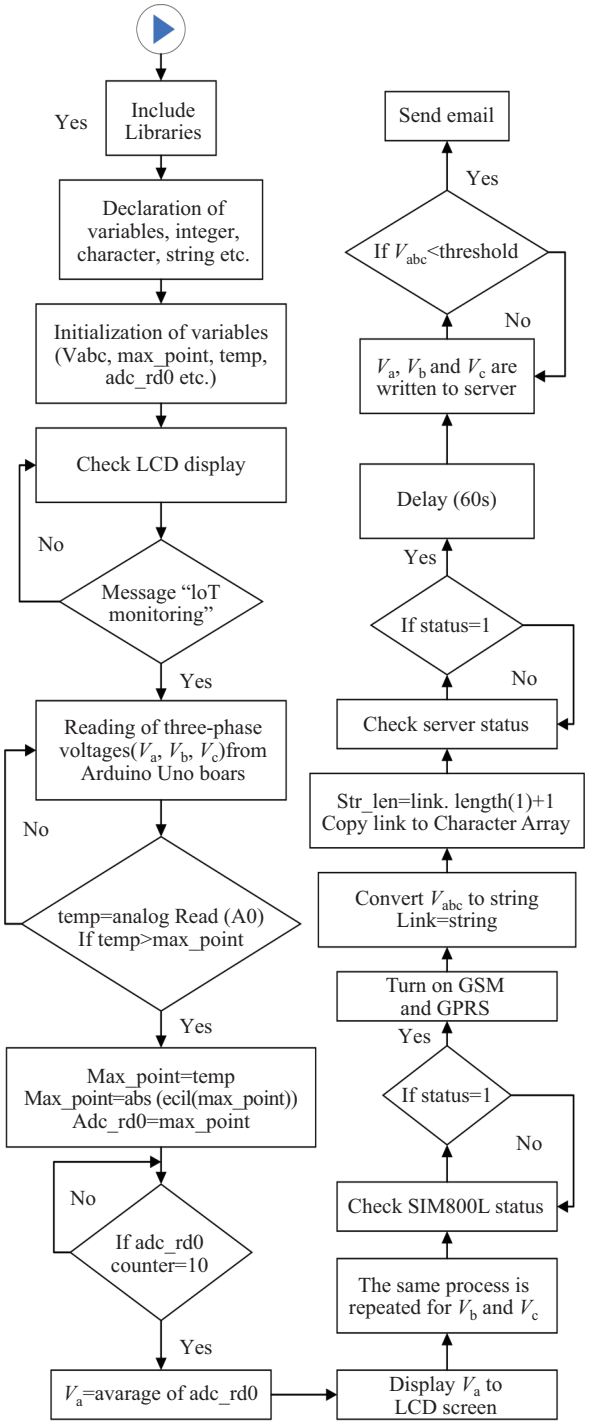

Fig. 7. A brief flow diagram of the proposed Industrial IoT for WECS.

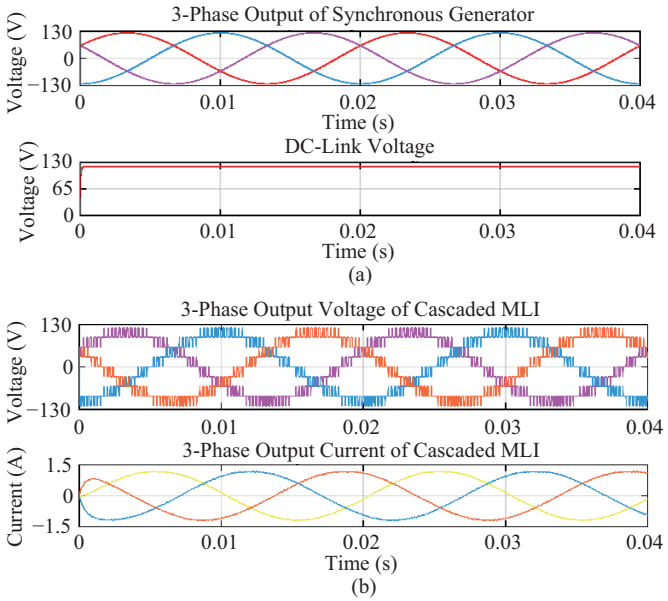

Fig. 8. (a) Synchronous generator three-phase voltages and DC-link voltage (b) three-phase output voltages and currents of the three-phase cascaded MLI.

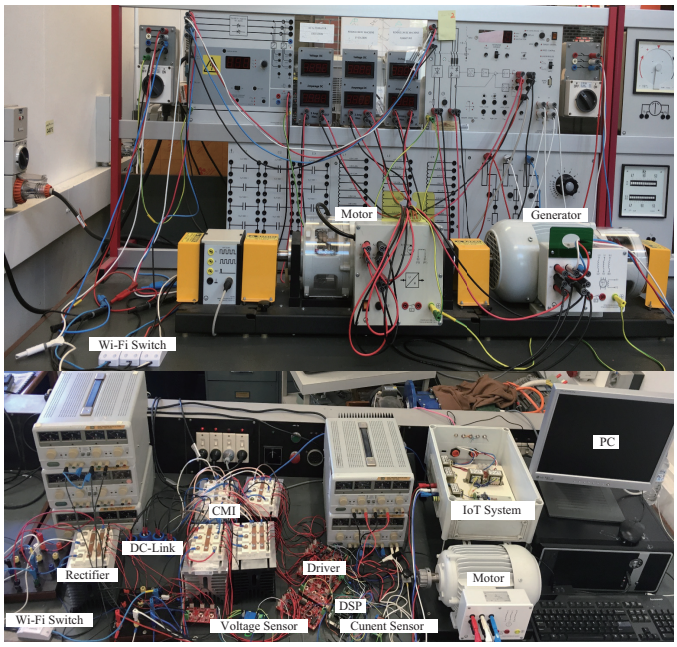

Fig. 9. Experimental setup of the proposed industrial internet of things for WECS.

digital signal processor (DSP) control board. DSP interface software (code composer studio, ccs 3.3) is employed to generate the controller source code from the Simulink model and transfers the source code to the DSP general purpose input/output (GPIO) pins. The DSP controller produces firing pulses of 3.3 V each, which are connected to isolated gate bipolar transistor (IGBT) gate driver modules to boost the voltage to 15 V. The output of the IGBT gate drivers are fed to the IGBT gate terminals (S_1 to S_6). The sensor module is connected to the AC/DC rectifier to capture the ripple voltage which is fed to the DSP board through analogue to digital conversion pins. The sensing and feedback block diagram for the complete processing of the signal is shown in Fig. 9.

The experimental output voltage of the AC/DC rectifier has been fed to the input of the CMLI. The proposed PI based SVPWM controller is applied to control the CMLI through DSP, following the same procedure as the AC/DC rectifier. The sensor module is connected to the CMLI to capture the output which is fed to the DSP board through analogue to digital conversion pins. The sensing and feedback block diagram for the complete processing of the signal is shown in Fig. 9.

The experimental three-phase voltages of the synchronous

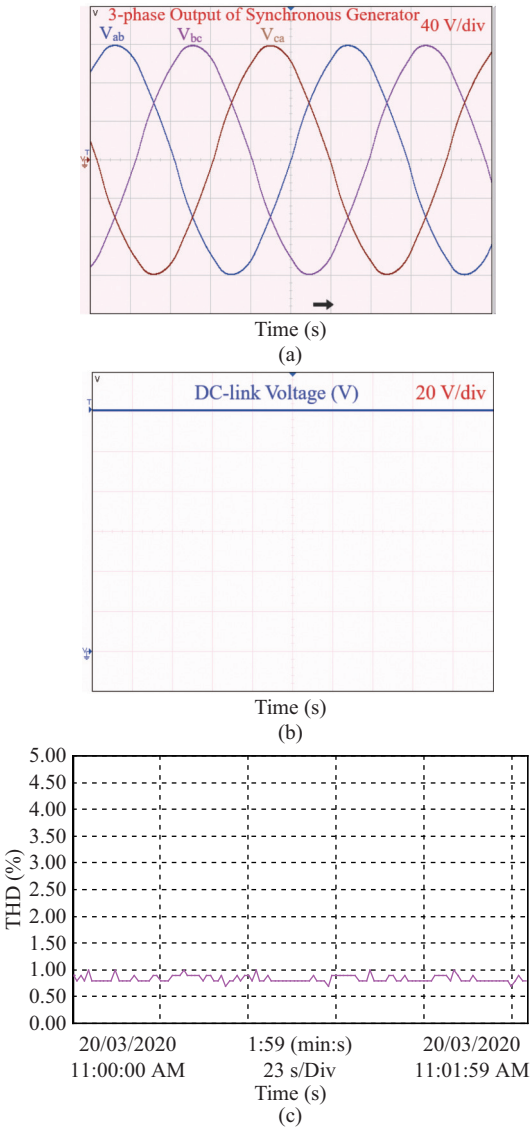

Fig. 10. Experimental results (a) synchronous generator three-phase voltages (b) DC-link voltage (c) voltage THD.

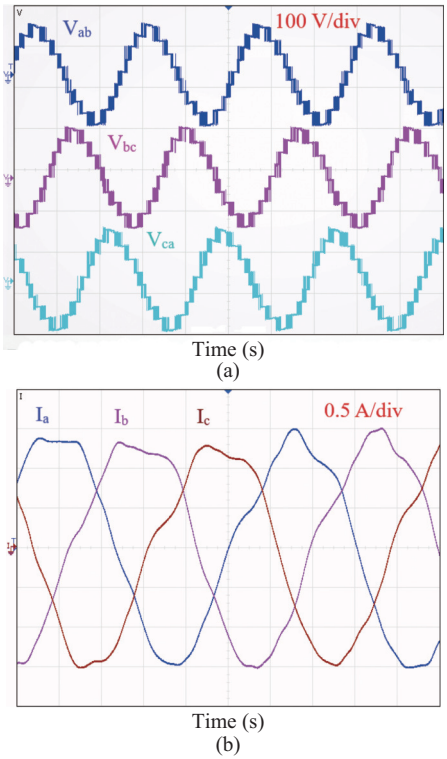

Fig. 11. Experimental results for the three-phase cascaded MLI (a) output voltage (b) output current.

generator and DC-link voltage are shown in Fig. 10 which are of the same trend as the simulation results. Total harmonic distortion (THD) of the generator voltage is less than 5% as depicted in Fig. 10(c) which satisfies the IEEE 519 standard.

The experimental three-phase voltages and currents of the three-phase cascaded MLI are presented in Fig. 11(a) and 11(b), espectively. As can be observed, the experimental results are in good agreement with the simulation results.

The proposed PI-based SVPWM embedded algorithm has been applied to monitor the condition of switching devices of the three-phase cascaded MLI and the three-phase output voltages are captured during faulty switches as depicted in Fig. 12.

Due to the switching fault, the output voltage waveforms (V_{ab} and V_{ca}) are affected as marked in Fig. 12 while V_{bc} is in a healthy condition. This indicates that the fault location is in either Phase-A or Phase-C switching devices. It can be observed that the positive peak of Phase-A and negative peak of Phase-C are affected which confirms the fault location to be within Phase-A not Phase-C. Furthermore, as the positive portion of phase-A is affected, the fault is expected to be within the upper switching devices (S_{a1} to S_{a4}) since the upper switching devices execute the positive level of the output voltages. It is to be noted that switching devices, S_{a1}, S_{a2}, S_{a3}, and S_{a4} take part in generating levels 2, 3, 4 and 5 of the output voltages, respectively. Results show that the fifth level of Phase-A is affected while other levels remain in normal conditions. It can be concluded that the fault location is within S_{a4} switch.

The condition of the DC-link capacitors has been monitored in the physical layer too by applying the proposed PI-based SVPWM embedded algorithm. Three-phase output voltage has been measured during the faulty DC-link capacitor as shown in Fig. 13. Due to such a fault, the output voltage is dropped to around 90 V and the 5^{th} level is wiped out. The abscence of the 5^{th} level of the three-phase voltage indicates a fault in the DC-link capacitors' (C_1 to C_4).

The condition of the switching devices (S_{a1} to S_{a4}) is monitored by combining the proposed PI-based SVPWM embedded algorithm and industrial IoT algorithm remotely in real time. The RMS of the MLI output voltage is presented in Fig. 14. The figure shows different modes of operation during healthy and faulty conditions. The healthy mode is shown in the first 30 s with an amplitude of around 76 V. When the fault takes place on S_{a1} at $t = 30$ s, the voltage drops down to around 73 V. When the fault is cleared at $t = 90$ s the voltage returns to a normal healthy level. The same process is repeated for all the upper switching devices of the MLI. The

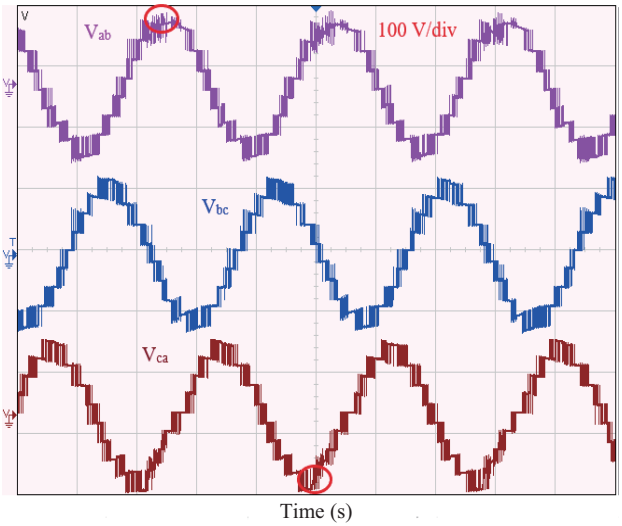

Fig. 12. Monitoring of faulty switching devices using the proposed PI-based SVPWM embedded algorithm.

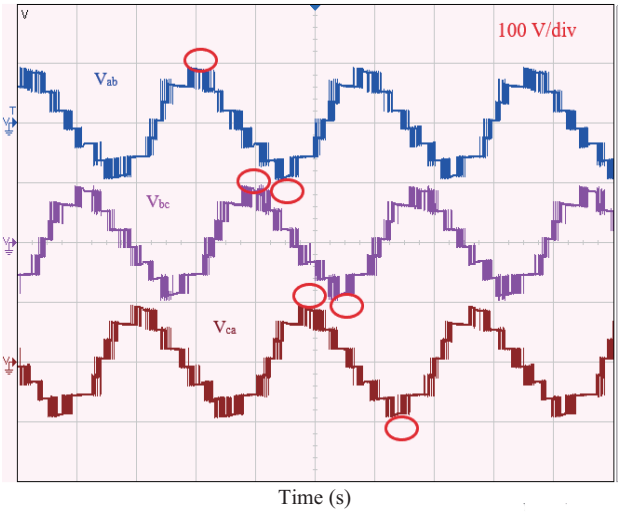

Fig. 13. DC-link capacitor faults monitoring using the proposed PI-based SVPWM embedded algorithm.

creation and clearance of faults are investigated over 270 s as shown in Fig. 14.

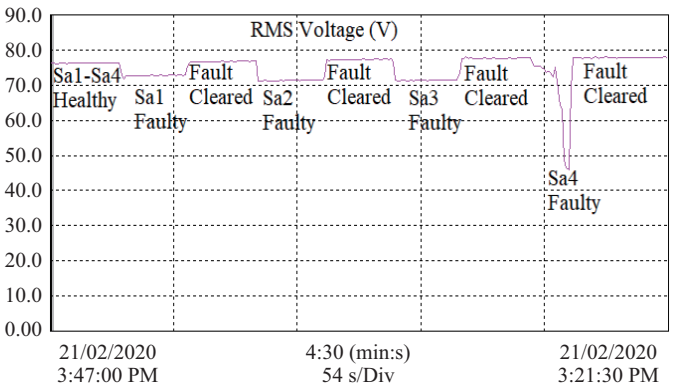

Fig. 14. Switching devices faults monitoring using industrial IoT.

The condition of the DC-link capacitors (C_1 to C_4) is also monitored through the proposed industrial IoT algorithm. The RMS of the MLI output voltage during DC-link capacitor faults is presented in Fig. 15. The DC-link capacitors are assumed to be healthy during the first 30 s and the amplitude of the voltage is around 76 V. When C_1 experiences an open circuit fault at $t = 30$ s, the RMS voltage is dropped to around 61 V whih lasts until the fault is cleared at $t = 90$ s over 270 s duration, as shown in Fig. 15.

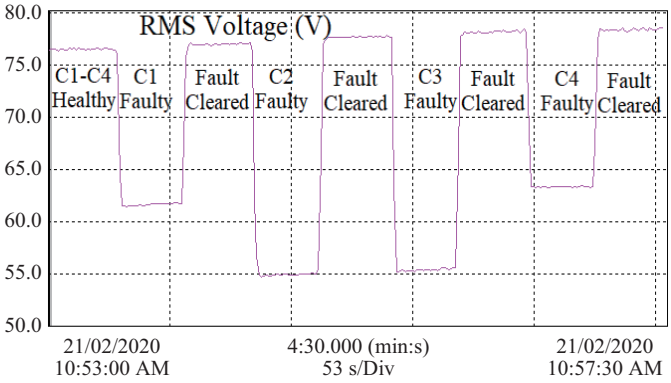

Fig. 15. DC-link capacitor faults monitoring using industrial IoT.

IV. Conclusion

This paper proposes a new PI-based SVPWM controller to suppress ripples and balance the DC-link voltages across the DC-link capacitors. An algorithm embedded into the PI-based SVPWM controller to monitor the condition of switching devices and DC-link capacitors in real-time has also been proposed. The PI-based SVPWM controller and the embedded algorithm have been designed and simulated in the MATLAB software environment. A hardware prototype has been developed to test the controller and embedded algorithm. Experimental and simulation results are found to be in good agreement. An industrial IoT algorithm and associated hardware prototype to monitor the condition of the switching devices and DC-link capacitors remotely in real-time is presented. In this way, authenticated remote users can monitor the conditions and take a proper and timely asset management decision to avoid any potential consequences to the WECS.

Acknowledgment

The first author would like to thank Curtin International Postgraduate Research Scholarship (CIPRS) and Curtin Strategic International Research Scholarship (CSIRS) program for supporting this research.

References

[1] A. Qazi, F. Hussain, N. Rahim, G. Hardaker, D. Alghazzawi, K. Shaban, and K. Haruna, "Towards sustainable energy: a systematic review of renewable energy sources, technologies, and public opinions," *IEEE Access*, vol. 7, pp. 63837–63851, May 2019.

[2] K. S. Rani,"'nvironmental effects of burning fossil fuels," *Journal of Chemical and Pharmaceutical Sciences*, Special Issue 3: Oct. 2014.

[3] A. Jahid, M. K. H. Monju, M. E. Hossain, and M. F. Hossain, "Renewable energy assisted cost aware sustainable off-grid base stations with energy cooperation," *IEEE Access*, vol. 6, pp. 60900–60920, Oct. 2018.

[4] BP Statistical Review of World Energy 2019: an unsustainable path, 68th edition, 2019, pp. 1–64.

[5] Renewable Capacity Statistics 2020, *International Renewable Energy Agency*, 2020, pp.1–60.

[6] "Wind power capacity worldwide reaches 597 GW, 50, 1 GW added in 2018," *World Wind Energy Agency*, Feb. 2019.

[7] "Clean Energy Australia Report 2019," *Clean Energy Council*, Apr. 2019, pp. 1–82.

[8] "Renewables Information: Overview," *International Energy Agency*, Aug. 2019.

[9] K. B. Tawfiq, A. S. Mansour, H. S. Ramadan, M. Becherif, and E. E. El-kholy, "Wind energy conversion system topologies and converters: comparative review," *Energy Procedia*, vol, 162, pp. 38–47, Apr. 2019.

[10] X. X. Yin and X. W. Zhao, "Composite hierarchical pitch angle control for a tidal turbine based on the uncertainty and disturbance estimator," *IEEE Transactions on Industrial Electronics*, vol. 67, no. 1, pp. 329–339, Jan. 2020.

[11] M. B. H. Kumar, B. Saravanan, P. Sanjeevikumar, and F. Blaabjerg, "Review on control techniques and methodologies for maximum power extraction from wind energy systems," *IET Renewable Power Generation*, vol. 12, no. 14, pp. 1609–1622, Oct. 2018.

[12] Z. B. Pan, F. Dong, J. W. Zhao, L. J. Wang, H. Wang, and Y. Y. Feng, "Combined resonant controller and two-degree-of-freedom PID controller for PMSLM current harmonics suppression," *IEEE Transactions on Industrial Electronics*, vol. 65, no. 9, pp. 7558–7568, Sep. 2018.

[13] A. Abu-Siada and S. Islam, "Application of SMES unit in improving the performance of an AC/DC power system," *IEEE Transactions on Sustainable Energy*, vol. 2, no. 2, pp. 109–121, Apr. 2011.

[14] M. A. Hannan, I. Hussin, P. J. Ker, M. M. Hoque, M. S. H. Lipu, A. Hussain, M. S. A. Rahman, and F. Blaabjerg, "Advanced control strategies of VSC based HVDC transmission system: issues and potential recommendations," *IEEE Access*, vol. 6, pp. 78352–78369, Dec. 2018.

[15] A. S. Gadalla, X. W. Yan, and H. Hasabelrasul, "Performance of the battery energy storage systems based on cascaded H-bridge multilevel converter," *The Journal of Engineering*, vol. 2019, no. 16, pp. 779–783, 2019.

[16] N. Mukherjee and D. Strickland, "Analysis and comparative study of different converter modes in modular second-life hybrid battery energy storage systems," *IEEE Journal of Emerging and Selected Topics in Power Electronics*, vol. 4, no. 2, pp. 547–563, Jun. 2016.

[17] M. J. Liu, W. Y. Li, C. S. Wang, M. P. Polis, L. Y. Wang, and J. Li, "Reliability evaluation of large scale battery energy storage systems," *IEEE Transactions on Smart Grid*, vol. 8, no. 6, pp. 2733–2743, Nov. 2017.

[18] Y. F. Shen, H. Wang, Z. Shen, Y. S. Yang, and F. Blaabjerg, "A 1-MHz series resonant DC–DC converter with a dual-mode rectifier for PV microinverters," *IEEE Transactions on Power Electronics*, vol. 34, no. 7, pp. 6544–6564, Jul. 2019.

[19] P. Garg, Priyanshi, and G. Bhuvaneswari, "Power electronic circuit based implementation of a solar PV emulator using a power factor corrected buck converter," in *2018 IEEMA Engineer Infinite Conference (eTechNxT)*, New Delhi, 2018, pp. 1–6.

[20] L. Zhao, Q. X. Ge, Z. D. Zhou, B. Yang, and Y. H. Li, "Research of high-power converter based on the wide band gap power semiconductor devices for rail transit electrical drive," in *2018 1st Workshop on Wide Bandgap Power Devices and Applications in Asia (WiPDA Asia)*, Xi'an, China, 2018, pp. 1–4.

[21] A. Ramya, M. Balaji, and C. Bharatiraja, "Power quality improvement in BLDC motor drive using Bridgeless Modified Cuk converter," in *2018 IEEE International Conference on Power Electronics, Drives and Energy Systems (PEDES)*, Chennai, India, 2018, pp. 1–6.

[22] Y. Rozanov, K. Kryukov, M. Kiselev, M. Lepanov, Y. Tserkovsky, and E. Namestnikova, "Power conditioning unit for direct-drive wave energy converter," in *2018 IEEE 18th International Power Electronics and Motion Control Conference (PEMC)*, Budapest, 2018, pp. 416–420.

[23] P. Drabek and L. Poljak, "Metods for voltage ripple mitigation on DC side of single-phase AC\DC converters," in *2015 International Conference on Applied Electronics (AE)*, Pilsen, 2015, pp. 201–204.

[24] X. N. Zhao, L. H. Zhang, R. Born, and J. S. Lai, "Solution of input double-line frequency ripple rejection for high-efficiency high-power density string inverter in photovoltaic application," in *2016 IEEE Applied Power Electronics Conference and Exposition (APEC)*, Long Beach, CA, 2016, pp. 1148–1154.

[25] M. Arias, I. Castro, D. G. Lamar, A. Vázquez, and J. Sebastián, "Optimized design of a high input-voltage-ripple-rejection converter for LED lighting," *IEEE Transactions on Power Electronics*, vol. 33, no. 6, pp. 5192–5205, Jun. 2018.

[26] P. Das, M. Pahlevaninezhad, J. Drobnik, G. Moschopoulos, and P. K. Jain, "A nonlinear controller based on a discrete energy function for an AC/DC boost PFC converter," *IEEE Transactions on Power Electronics*, vol. 28, no. 12, pp. 5458–5476, Dec. 2013.

[27] B. Veerasamy, W. Kitagawa, and T. Takeshita, "Output ripple minimization of single-stage power factor corrected bi-directional buck AC/DC converter," in *2014 International Power Electronics Conference (IPEC-Hiroshima 2014-ECCE ASIA)*, Hiroshima, 2014, pp. 2310–2317.

[28] Jé Rodríguez, J. S. Lai, F. Z. Peng, "Multilevel inverters: a survey of topologies, controls, and applications," *IEEE Transactions on Industrial Electronics*, vol. 49, no. 4, pp. 724–738, Aug, 2002.

[29] R. Mishra and V. Agarwal, "Novel voltage balancing techniques for modular multilevel PV inverters," in *2018 IEEE Industry Applications Society Annual Meeting (IAS)*, Portland, OR, 2018, pp. 1–8.

[30] O. V. Nos, S. V. Brovanov, S. A. Kharitonov, P. N. Smirnov, and E. E. Abramushkina, "The capacitor voltage balancing of cascaded h-bridge multilevel inverter," in *2019 IEEE International Conference on Mechatronics (ICM)*, Ilmenau, Germany, 2019, pp. 327–331.

[31] K. Anuradha and G. R. Krishna, "Neutral point voltage level stabilization and DC link capacitors voltage balance in neutral point clamped multilevel inverters," in *2016 11th International Conference on Industrial and Information Systems (ICIIS)*, Roorkee, 2016, pp. 838–843.

[32] K. Ma, H. Wang, and F. Blaabjerg, "New approaches to reliability assessment: using physics-of-failure for prediction and design in power electronics systems," *IEEE Power Electronics Magazine*, vol. 3, no. 4, pp. 28–41, Dec. 2016.

[33] H. Soliman, H. Wang, and F. Blaabjerg, "A review of the condition monitoring of capacitors in power electronic converters," *IEEE Transactions on Industry Applications*, vol. 52, no. 6, pp. 4976–4989, Nov. /Dec. 2016.

[34] E. Wolfgang, "Examples for failures in power electronics systems," in *Procedings ECPE Tutorial Reliability of Power Elec-tronic Systems*, Nuremberg, Germany, 2007, pp. 19–20.

[35] M. L. Hossain, Abu-Siada, M. Muyeen, "Methods for advanced wind turbine condition monitoring and early diagnosis: a literature review," *Energies*, vol. 11, no. 5, pp. 1309, May 2018.

[36] I. Miladinovic and S. Schefer-Wenzl, "NFV enabled IoT architecture for an operating room environment," in *IEEE 4th World Forum on Internet of Things (WF-IoT)*, Singapore, 2018, pp. 98–102.

[37] "IDC forecasts worldwide spending on the internet of things," *International Data Corporation*, 2019.

[38] Y. X. Liao, E. de Freitas Rocha Loures, and F. Deschamps, "Industrial internet of things: a systematic literature review and insights," *IEEE Internet of Things Journal*, vol. 5, no. 6, pp. 4515–4525, Dec. 2018.

[39] The Industrial Internet of Things, Connectivity Framework, Industrial Internet Consortium, vol. G5, 2018.

[40] Z. B. Ibrahim, M. L. Hossain, I. B. Bugis, N. M. N. Mahadi, and A. S. A. Hasim, "Simulation investigation of SPWM, THIPWM and SVPWM techniques for three phase voltage source inverter", *International Journal of Power Electronics and Drive Systems*, vol.6, no.2, Jun. 2014.

[41] Z. B. Ibrahim, M. L. Hossain, I. B. Bugis, J. M. Lazi, and N. M. Yaakop, "Three level diode clamped inverter based on space vector pulse width modulation technique," *International Journal of Power Electronics and Drive Systems*, vol. 4, no. 1B, Jul. 2014.

Md. Liton Hossain received his Bachelor of Science degree in Electrical and Electronic Engineering in 2012 from Khulna University of Engineering & Technology, Bangladesh. He also acquired his Master of Science degree in Electrical Engineering from Universiti Teknikal Malaysia Melaka in 2016. Currently, he is pursuing his PhD degree at Curtin University, Australia. His current research interests include industrial internet of things, wind energy conversion systems, renewable energy, power electronic converters, multilevel inverter, motor drive and solar cell.

Ahmed Abu-Siada received his B.Sc. and M.Sc. degrees from Ain Shams University, Cairo, Egypt, in 1998, and his Ph.D. degree from Curtin University, Perth, WA, Australia, in 2004, all in electrical engineering. He is currently the Discipline lead of Electrical and Computer Engineering, Curtin University. Dr. Abu-Siada is the Editor-in-Chief of the International Journal of Electrical and Electronic Engineering and regular Reviewer for various IEEE transactions. He is the Vice Chair of the IEEE Computation Intelligence Society, WA Chapter. His research interests include power system stability, condition monitoring, power electronics, and power quality.

S M Muyeen received his B.Sc.Eng. degree from the Rajshahi Institute of Technology, Bangladesh, in 2000, and his M.Eng. and Ph.D. degrees from the Kitami Institute of Technology, Japan, in 2005 and 2008, respectively, all in electrical and electronic engineering. He is currently an Associate Professor with the Department of Electrical and Computer Engineering, Curtin University, Perth, WA, Australia. He has published more than 175 articles in different journals and international conferences. He has published six books as an author or an editor. He has been a Keynote Speaker and an Invited Speaker at many international conferences, workshops, and universities. He serves as an Editor/an Associate Editor for many prestigious journals of IEEE, IET, and other publishers, including the IEEE Transactions of Sustainable Energy, the IEEE Power Engineering Letters, IET Renewable Power Generation, and IET Generation, Transmission and Distribution. He is a Fellow of the Engineers Australia. His research interests include power system stability and control, electrical machine, FACTS, energy storage systems (ESS), renewable energy, and HVDC systems.

Md Mubashwar Hasan received his PhD degree in electrical engineering from Curtin University, Perth, WA, Australia in 2018. He is currently working as a research associate in the School of Science, Engineering and IT, Federation University, Australia. His research interests include high power converters, efficient renewable power conditioning techniques and compact electric transformer.

Md Momtazur Rahman is currently a PhD student working with Professor Kamal Alameh at Edith Cowan University (ECU), Australia. His doctoral research at ECU focuses on development of solar energy-harvesting technologies for greenhouse applications. He takes a multidisciplinary approach that encompasses the fields of Electrical Engineering, Material Science and Renewable Energy. He is also an Assistant Professor at the Bangladesh Army University of Engineering & Technology (BAUET), on study leave. He holds Bachelor's and Master's degrees in Electrical & Electronic Engineering (EEE), and Energy Science & Technology (EST) from Khulna University of Engineering & Technology (KUET), Bangladesh and the University of Ulm, Germany. He was a student member of the Institute of Electrical and Electronics Engineers (IEEE), USA.